IEEE Access
Multidisciplinary | Rapid Review | Open Access Journal

Received December 21, 2020, accepted December 22, 2020, date of publication December 25, 2020,
date of current version January 6, 2021.

Digital Object Identifier 10.1109/ACCESS.2020.3047485

Analysis and Experiment on Multi-Antenna-to-Multi-Antenna RF Wireless Power Transfer

JE HYEON PARK, (Student Member, IEEE), DONG IN KIM, (Fellow, IEEE), AND KAE WON CHOI, (Senior Member, IEEE)
Department of Electrical and Computer Engineering, College of Information and Communication Engineering, Sungkyunkwan University, Suwon 16419, South Korea

Corresponding author: Kae Won Choi (kaewonchoi@skku.edu)

This work was supported in part by the National Research Foundation of Korea (NRF) funded by the Ministry of Science, ICT and Future Planning (MSIP), Korean Government under Grant 2014R1A5A1011478, and in part by the Basic Science Research Program through the National Research Foundation of Korea (NRF) funded by the Korean Government (MSIP) under Grant NRF-2020R1A2C1014693.

ABSTRACT In this paper, we provide a tool for predicting the power transfer efficiency of radio-frequency (RF) wireless power transfer (WPT). With its capability of long-range wireless power transfer, RF WPT is considered as a very promising recharging technique for powering low-power internet of things (IoT) devices. The prediction of the power transfer efficiency is a prerequisite for setting up a proper design goal of RF WPT systems. We propose an analytic method that enables to calculate the efficiency in various multi-antenna-to-multi-antenna WPT scenarios with arbitrary positions and attitudes of antenna arrays. We have built a prototype RF WPT system with 64 transmit and 16 receive antennas, the operating frequency of which is 5.8 GHz, and verified the accuracy of the proposed analysis.

INDEX TERMS RF wireless power transfer, microwave power transfer, beam efficiency, phased antenna array.

I. INTRODUCTION

Recently, radio-frequency (RF) wireless power transfer (WPT) has gained a great momentum [1]. Unlike the inductive or resonant coupling-based near-field WPT, RF WPT is capable of long-range wireless power transfer by the radiation of the electromagnetic (EM) waves. Due to its characteristics, RF WPT is especially suitable for powering up low-power digital devices scattered over a wide area.

The internet of things (IoT) is expected to be a key enabling technology of the next industrial revolution. However, massive deployment of the low-power IoT devices in smart factories, warehouses, and buildings will pose a new challenge of extending the lifetime of such IoT devices. The RF WPT has a potential to solve this problem by wirelessly supplying power and removing the necessity of battery replacement or wired power cords [2].

There have been a number of research works investigating various aspects of RF WPT. The efforts to enhance the RF-to-DC conversion efficiency of the rectifier have been pursued, for example, [3] proposes a GaN Schottky barrier diode for high-power RF WPT and [4] demonstrates the cooperate power harvester in which the DC bias voltage from the thermal source improves the RF-to-DC conversion efficiency. In addition, [5] has implemented electrically small single-substrate Huygens dipole rectenna which is suitable for IoT devices with ultra compact, lightweight, and low cost design. However, the RF-to-DC conversion is not a critical factor that determines the end-to-end RF WPT efficiency since most of the power loss arises while the EM wave propagates through the air.

The power transfer efficiency through the air is typically low because of the dispersive nature of free-space EM wave. Therefore, to enhance the efficiency, a sufficiently large transmit aperture should focus the EM wave on to the receiver which is also large enough to capture as much EM wave as possible. The antenna array system with multiple transmit and receive antennas can implement such a large aperture WPT system [6]. For example, the retrodirective antenna arrays have been proposed in [7] and [8], and the beam synthesis for achieving the maximum efficiency is studied in [9]. Some works have demonstrated the multi-antenna-to-multi-antenna RF WPT system for charging low-power devices (e.g., [10]–[12]). Main focus of these works is the

The associate editor coordinating the review of this manuscript and approving it for publication was Giorgio Montisci.

demonstration of the full-fledged RF WPT systems including the RF and control circuits as well as tracking algorithms, but they do not give in-depth investigation into the working principle behind RF WPT.

In this paper, we analyze the power transfer efficiency of the multi-antenna-to-multi-antenna RF WPT system, and provide experimental results obtained from the prototype phased-array WPT system to verify the analytic results. The analysis on the power transfer efficiency has a practical importance as well as a theoretical value. The power transfer efficiency depends not only on the hardware specification (e.g., the number of transmit and receive antennas) but also on the positions and attitudes of the transmitter and receiver due to the power attenuation, antenna gain, and polarization. For example, suppose that an engineer attempts to design an RF WPT system for charging sensors on production lines from the WPT transmitter installed at the ceiling in a smart factory. The engineer has to be able to predict the power transfer efficiency for all possible positions and attitudes of the receiver so that a proper system design goal is set up.

Currently, there is no readily available method to effectively predict the power transfer efficiency. The RF WPT should work within the radiative near field region to achieve a reasonable power transfer efficiency. This is because a transmitter is able to focus the EM wave beam on to a small spot within the radiative near field region like the convex lens does [13]–[16]. Therefore, a simple Friis equation for calculating a free space loss in the far-field region cannot be applied to the RF WPT. Moreover, the full wave EM simulation takes too much time and memory to compute radiation within a radiative near field.

There have been a few papers analyzing the RF WPT efficiency, e.g., [17] and [18]. In [17], the efficiency is analyzed for RF WPT from and to continuous apertures facing to each other. On the other hand, the authors of [18] have made use of the reciprocity theorem to analyze the efficiency from a continuous aperture to a single mobile antenna. However, these works cannot be used for analyzing a practical multi-antenna WPT since they assume a fictitious continuous aperture transmitter or receiver. Moreover, the method for the efficiency computation in a general scenario is not given, and the computational complexity is very high since an integral or eigendecomposition over a continuous aperture is involved.

The multiple-input multiple-output (MIMO) antenna-based analysis and optimization from the perspective of wireless communications have been proposed by a number of papers (e.g., [19], [20]). These works focus on optimizing the transmitting signal and beamforming weights given that the power transfer characteristics are modeled as statistical fading communication channels. While this statistical fading channel model is suitable for describing the wireless communications scenario, it has several limitations in modeling the RF WPT. The statistical fading channel model is valid only when there is complex radio environments with many scatterers between sufficiently separated transmitter and receiver. However, in this situation, the power transfer efficiency is extremely low in general and the useful amount of power cannot be provided to the receiver. Moreover, the analysis based on the statistical fading channel model does not consider critical factors determining the power transfer efficiency such as the attitude, radiation pattern, polarization, and mutual coupling of the transmit and receive antenna arrays, and therefore, it cannot answer even to a seemingly simple question: what is the power transfer efficiency between freely positioned antenna arrays?

In our proposed analysis, the transmit and receive antenna arrays can be freely located in the three-dimensional space with arbitrary attitudes as seen in Fig. 1(a). The radiation pattern and polarization of the antenna elements as well as the mutual coupling within the antenna arrays are all considered in a unified way so that the power transfer efficiency of the practical RF WPT system is correctly derived. We analyze the impedance matrix between the all antenna ports, and cast the RF WPT model into the multi-port-to-multi-port power transfer model as in Fig. 1(b). We obtain the optimal excitation of each antenna port, based on which the power transfer efficiency is calculated. The proposed method is practically

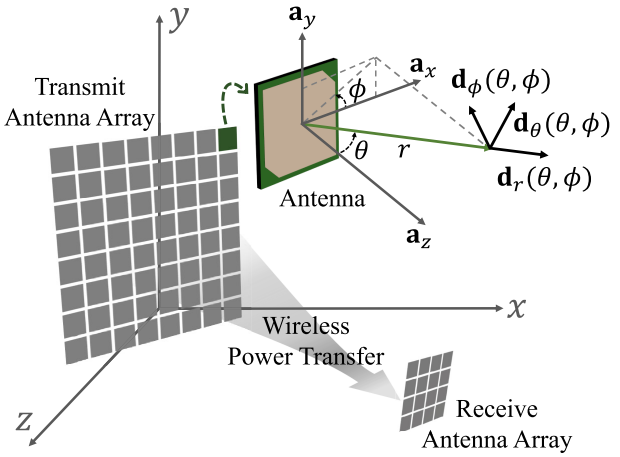

(a) Position and attitude of antenna arrays

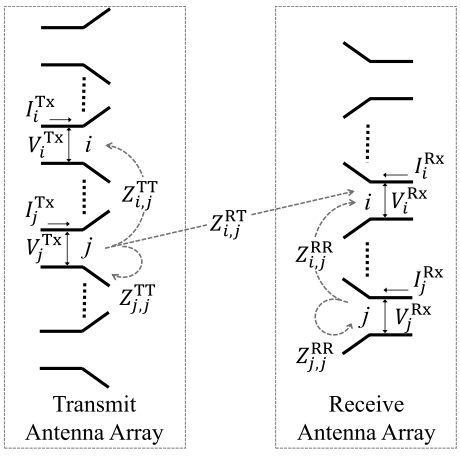

(b) Antenna port model

FIGURE 1. Multi-antenna-to-multi-antenna RF WPT model.

useful in that the efficiency can be computed in any deployment scenario with very low computational overhead.

In this paper, we have implemented a prototype phased-array WPT systems to experimentally verify the accuracy of the proposed analysis. The implemented WPT systems work on 5.8 GHz ISM bands, which are equipped with 64 transmit antennas and 16 receive antennas. To the best of our knowledge, the experimental validation of the analytic results of the multi-antenna WPT has not been done by any previous work.

In summary, the novel contributions of this paper is as follows.

- We have developed an analysis method for the practical multi-antenna to multi-antenna RF WPT in the radiative near field region. The existing Friis equation cannot explain the WPT within the radiative near field region. Moreover, the theoretical analysis in the previous works assumes a fictitious continuous aperture, which cannot predict the power transfer efficiency of the real multi-antenna WPT systems.
- The proposed analysis method can analyze the RF WPT scenario where the transmitter and receiver are freely located in the three-dimensional space with the full consideration of the radiation pattern, polarization, and mutual coupling of antenna elements. None of the existing method can analyze such scenario.
- The validity of the propose method is verified by the full-wave simulation as well as the real experiments.

The rest of the paper is organized as follows. Section II explains the RF WPT system model. The RF WPT is analyzed in Section III, and the analytic results are verified by the experiments in Section IV. The paper is concluded with Section V.

II. RF WIRELESS POWER TRANSFER SYSTEM MODEL

A. POSITION AND ATTITUDE OF ANTENNA ARRAY

We consider a point-to-point RF WPT system that consists of a transmitter and a receiver. The transmitter sends a continuous wave (CW) of frequency f to the receiver for WPT. Both the transmitter and receiver utilize antenna arrays for transmitting and receiving an EM wave.

The transmitter and receiver are equipped with antenna arrays, which consist of N^{Tx} and N^{Rx} antennas, respectively. The nth antenna of the transmit antenna array will be called tx-antenna n. Likewise, the nth antenna of the receive antenna array will be called rx-antenna n.

Each antenna constituting the transmit and receive antenna arrays can be freely located in a global Cartesian coordinate system with the x, y, and z axes. The three-dimensional positions of the phase centers of tx-antenna n and rx-antenna m are denoted by the column vectors $\mathbf{q}_n^{\mathrm{Tx}} = (q_{n,x}^{\mathrm{Tx}}, q_{n,y}^{\mathrm{Tx}}, q_{n,z}^{\mathrm{Tx}})^T$ and $\mathbf{q}_m^{\mathrm{Rx}} = (q_{m,x}^{\mathrm{Rx}}, q_{m,y}^{\mathrm{Rx}}, q_{m,z}^{\mathrm{Rx}})^T$, respectively.

The attitude of each antenna is decided by the antenna frame represented by three orthogonal axes as shown in Fig. 1(a). The three axes of the antenna frame of tx-antenna n are the three-dimensional column vectors $\mathbf{a}_{n,x}^{\mathrm{Tx}}$, $\mathbf{a}_{n,y}^{\mathrm{Tx}}$, and $\mathbf{a}_{n,z}^{\mathrm{Tx}}$. Then, the antenna frame of tx-antenna n is completely defined by the 3×3 matrix $\mathbf{A}_n^{\mathrm{Tx}} = (\mathbf{a}_{n,x}^{\mathrm{Tx}}, \mathbf{a}_{n,y}^{\mathrm{Tx}}, \mathbf{a}_{n,z}^{\mathrm{Tx}})$. We will call $\mathbf{A}_n^{\mathrm{Tx}}$ the antenna frame of tx-antenna n. Similarly, we define $\mathbf{A}_n^{\mathrm{Rx}} = (\mathbf{a}_{n,x}^{\mathrm{Rx}}, \mathbf{a}_{n,y}^{\mathrm{Rx}}, \mathbf{a}_{n,z}^{\mathrm{Rx}})$ as the antenna frame of rx-antenna n.

We can view $\mathbf{A}_n^{\mathrm{Tx}}$ and $\mathbf{A}_n^{\mathrm{Rx}}$ as the rotation matrix that rotates the antenna together with the corresponding antenna frame, the axes of which are initially aligned with the x, y, and z axes of the global Cartesian coordinate system. One intuitive way to represent the rotation is the Euler angle. The rotation matrices that represent the rotation of α, β, and γ around x, y, and z axes of the global Cartesian coordinate system are respectively given by

$$\mathbf{R}_x(\alpha) = \begin{bmatrix} 1 & 0 & 0 \\ 0 & \cos\alpha & -\sin\alpha \\ 0 & \sin\alpha & \cos\alpha \end{bmatrix},$$
$$\mathbf{R}_y(\beta) = \begin{bmatrix} \cos\beta & 0 & \sin\beta \\ 0 & 1 & 0 \\ -\sin\beta & 0 & \cos\beta \end{bmatrix},$$
$$\mathbf{R}_z(\gamma) = \begin{bmatrix} \cos\gamma & -\sin\gamma & 0 \\ \sin\gamma & \cos\gamma & 0 \\ 0 & 0 & 1 \end{bmatrix}. \quad (1)$$

For example, suppose that the antenna frame of tx-antenna n is first aligned with the global Cartesian coordinate system and is then rotated by an Euler angle (α, β, γ) with the x-y'-z'' intrinsic rotation convention. Then, the antenna frame $\mathbf{A}_n^{\mathrm{Tx}}$ of the antenna is given by

$$\mathbf{A}_n^{\mathrm{Tx}} = \mathbf{R}_x(\alpha)\mathbf{R}_y(\beta)\mathbf{R}_z(\gamma). \quad (2)$$

B. IMPEDANCE MATRIX AT ANTENNA PORTS

In this subsection, we explain the antenna port model, shown in Fig. 1(b). The voltage and current at the port of tx-antenna n are denoted by V_n^{Tx} and I_n^{Tx}, respectively. Similarly, the voltage and current at the port of rx-antenna m are denoted by V_m^{Rx} and I_m^{Rx}, respectively. The column vectors of the voltages and currents at the ports of antenna elements are defined as $\mathbf{V}^{\mathrm{Tx}} = (V_1^{\mathrm{Tx}}, \ldots, V_{N^{\mathrm{Tx}}}^{\mathrm{Tx}})^T$, $\mathbf{I}^{\mathrm{Tx}} = (I_1^{\mathrm{Tx}}, \ldots, I_{N^{\mathrm{Tx}}}^{\mathrm{Tx}})^T$, $\mathbf{V}^{\mathrm{Rx}} = (V_1^{\mathrm{Rx}}, \ldots, V_{N^{\mathrm{Rx}}}^{\mathrm{Rx}})^T$, and $\mathbf{I}^{\mathrm{Rx}} = (I_1^{\mathrm{Rx}}, \ldots, I_{N^{\mathrm{Rx}}}^{\mathrm{Rx}})^T$.

The radiation impedances of tx-antenna i and rx-antenna j are denoted by $Z_{i,i}^{\mathrm{TT}}$ and $Z_{j,j}^{\mathrm{RR}}$, respectively. We consider the mutual coupling between the antennas in the transmit and receive antenna arrays. The mutual impedance $Z_{i,j}^{\mathrm{TT}}$ for $i \neq j$ of the transmit antenna array is defined as the ratio of the voltage at the open-circuit port of tx-antenna i to the current excited at the port of tx-antenna j. The mutual impedance for the receive antenna array is denoted by $Z_{i,j}^{\mathrm{RR}}$ for $i \neq j$. The impedance matrices of the transmit and receive antenna arrays are defined as an N^{Tx}-by-N^{Tx} matrix $\mathbf{Z}^{\mathrm{TT}} = [Z_{i,j}^{\mathrm{TT}}]$ and an N^{Rx}-by-N^{Rx} matrix $\mathbf{Z}^{\mathrm{RR}} = [Z_{i,j}^{\mathrm{RR}}]$, respectively.

The radiated EM wave excited from the current at the port of tx-antenna j induces a voltage at the open-circuit port of rx-antenna i. The impedance $Z_{i,j}^{\mathrm{RT}}$ is defined as the ratio of such voltage to the current. The impedance matrix from the

transmit to receive antenna arrays is defined as an N^{Rx}-by-N^{Tx} matrix $\mathbf{Z}^{\mathrm{RT}} = [Z^{\mathrm{RT}}_{i,j}]$. Similarly, the impedance matrix from the receive to transmit antenna arrays is defined as an N^{Tx}-by-N^{Rx} matrix $\mathbf{Z}^{\mathrm{TR}} = [Z^{\mathrm{TR}}_{i,j}]$. We have $\mathbf{Z}^{\mathrm{TR}} = (\mathbf{Z}^{\mathrm{RT}})^T$ due to the reciprocity.

The current-voltage relationship between all antenna ports is fully described by the following formula.

$$\begin{bmatrix} \mathbf{V}^{\mathrm{Tx}} \\ \mathbf{V}^{\mathrm{Rx}} \end{bmatrix} = \begin{bmatrix} \mathbf{Z}^{\mathrm{TT}} & \mathbf{Z}^{\mathrm{TR}} \\ \mathbf{Z}^{\mathrm{RT}} & \mathbf{Z}^{\mathrm{RR}} \end{bmatrix} \begin{bmatrix} \mathbf{I}^{\mathrm{Tx}} \\ \mathbf{I}^{\mathrm{Rx}} \end{bmatrix}. \tag{3}$$

C. MUTUAL IMPEDANCE MATRIX AND RADIATION PATTERN

In this analysis, we assume that the mutual impedance matrices of the transmit and receive antenna arrays, i.e., $\mathbf{Z}^{\mathrm{TT}}$ and $\mathbf{Z}^{\mathrm{RR}}$, are known in advance. The full-wave simulation or the network analyzer measurements of the antenna array can provide these mutual impedance matrices.

The radiation pattern of each individual antenna is known in advance as well by means of the full-wave simulation or the radiation pattern measurements. The radiation pattern is an embedded pattern obtained by exciting one antenna of interest with a unit current while all the other antenna ports are open. The radiation pattern is given as the E-field pattern in two orthogonal axes (i.e., elevation and azimuth axes) for each direction. Suppose that the radiation direction is given by elevation θ and azimuth ϕ. Then, the E-field pattern of tx-antenna n is denoted by $\Omega^{\mathrm{Tx}}_{n,\theta}(\theta,\phi)$ and $\Omega^{\mathrm{Tx}}_{n,\phi}(\theta,\phi)$ on the elevation and azimuth axes, respectively.

From the E-field pattern, the E-field at distance r is given by

$$E^{\mathrm{Tx}}_{n,\theta}(r,\theta,\phi) = \Omega^{\mathrm{Tx}}_{n,\theta}(\theta,\phi)\cdot\frac{1}{r}\exp(-jkr)\cdot I^{\mathrm{Tx}}_n, \tag{4}$$

$$E^{\mathrm{Tx}}_{n,\phi}(r,\theta,\phi) = \Omega^{\mathrm{Tx}}_{n,\phi}(\theta,\phi)\cdot\frac{1}{r}\exp(-jkr)\cdot I^{\mathrm{Tx}}_n, \tag{5}$$

where $E^{\mathrm{Tx}}_{n,\theta}(r,\theta,\phi)$ and $E^{\mathrm{Tx}}_{n,\phi}(r,\theta,\phi)$ are the E-fields on the elevation and azimuth axes, respectively, and k is the free-space wavenumber.

Likewise, the E-field pattern of rx-antenna n is denoted by $\Omega^{\mathrm{Rx}}_{n,\theta}(\theta,\phi)$ and $\Omega^{\mathrm{Rx}}_{n,\phi}(\theta,\phi)$ on the elevation and azimuth axes, respectively. This E-field pattern for a receive antenna has the same definition with the one for a transmit antenna. We will use the E-field pattern for a receive antenna to obtain the effective length to calculate the voltage excitation given the incident plane wave in Section II-E.

D. ANTENNA RADIATION MODEL

In this subsection, we first define the radiated EM wave from each transmit antenna when the antenna port is excited by a given current. We consider a spherical coordinate system within the antenna frame of tx-antenna n, and focus on the EM wave radiation towards the direction of elevation θ and azimuth ϕ, as in Fig. 1(a). Let us define a radiation frame as the 3×3 matrix $\mathbf{D}^{\mathrm{Tx}}_n(\theta,\phi) = (\mathbf{d}^{\mathrm{Tx}}_{n,\theta}(\theta,\phi), \mathbf{d}^{\mathrm{Tx}}_{n,\phi}(\theta,\phi), \mathbf{d}^{\mathrm{Tx}}_{n,r}(\theta,\phi))$, where $\mathbf{d}^{\mathrm{Tx}}_{n,\theta}(\theta,\phi)$, $\mathbf{d}^{\mathrm{Tx}}_{n,\phi}(\theta,\phi)$, and $\mathbf{d}^{\mathrm{Tx}}_{n,r}(\theta,\phi)$ are three-dimensional column vectors representing the three axes of the radiation frame. In the radiation frame, the EM wave propagates towards the direction of $\mathbf{d}^{\mathrm{Tx}}_{n,r}(\theta,\phi)$, and $\mathbf{d}^{\mathrm{Tx}}_{n,\theta}(\theta,\phi)$ and $\mathbf{d}^{\mathrm{Tx}}_{n,\phi}(\theta,\phi)$ are the elevation and azimuth axes, respectively.

The radiation frame $\mathbf{D}^{\mathrm{Tx}}_n(\theta,\phi)$ is equal to the z-y-z extrinsic rotation of the antenna frame $\mathbf{A}^{\mathrm{Tx}}_n$ by an Euler angle $(0,\theta,\phi)$. That is, $\mathbf{D}^{\mathrm{Tx}}_n(\theta,\phi)$ is obtained by rotating $\mathbf{A}^{\mathrm{Tx}}_n$ by θ around $\mathbf{a}^{\mathrm{Tx}}_{n,y}$ and by ϕ around $\mathbf{a}^{\mathrm{Tx}}_{n,z}$. Then, the radiation frame $\mathbf{D}^{\mathrm{Tx}}_n(\theta,\phi)$ is given by

$$\mathbf{D}^{\mathrm{Tx}}_n(\theta,\phi) = \mathbf{A}^{\mathrm{Tx}}_n\mathbf{R}_z(\phi)\mathbf{R}_y(\theta). \tag{6}$$

We calculate the E-field at distance r towards the propagation direction $\mathbf{d}^{\mathrm{Tx}}_{n,r}(\theta,\phi)$ from the phase center of tx-antenna n (i.e., $\mathbf{q}^{\mathrm{Tx}}_n$). That is, we derive the E-field of the EM wave at coordinate $\mathbf{q} = \mathbf{q}^{\mathrm{Tx}}_n + r\mathbf{d}^{\mathrm{Tx}}_{n,r}(\theta,\phi)$, which is induced by current I^{Tx}_n at the port of tx-antenna n as follows. From (4) and (5), we have

$$\begin{aligned}\mathbf{E}^{\mathrm{W}}_n(\mathbf{q}) &= \mathbf{D}^{\mathrm{Tx}}_n(\theta,\phi)\mathbf{E}^{\mathrm{Tx}}_n(r,\theta,\phi)\\ &= \mathbf{D}^{\mathrm{Tx}}_n(\theta,\phi)\boldsymbol{\Omega}^{\mathrm{Tx}}_n(\theta,\phi)\cdot\frac{1}{r}\exp(-jkr)\cdot I^{\mathrm{Tx}}_n,\end{aligned} \tag{7}$$

where $\mathbf{E}^{\mathrm{Tx}}_n(r,\theta,\phi) = (E^{\mathrm{Tx}}_{n,\theta}(r,\theta,\phi), E^{\mathrm{Tx}}_{n,\phi}(r,\theta,\phi), 0)^T$ and $\boldsymbol{\Omega}^{\mathrm{Tx}}_n(\theta,\phi) = (\Omega^{\mathrm{Tx}}_{n,\theta}(\theta,\phi), \Omega^{\mathrm{Tx}}_{n,\phi}(\theta,\phi), 0)^T$.

E. ANTENNA RECEPTION MODEL

In this subsection, we will derive the voltage excitation of a receive antenna when an incident plane wave comes to the receive antenna. We define a radiation frame of rx-antenna n to describe the incident plane wave. When the incident plane wave propagates towards the direction of elevation θ and azimuth ϕ, the radiation frame is defined as $\mathbf{D}^{\mathrm{Rx}}_n(\theta,\phi) = (\mathbf{d}^{\mathrm{Rx}}_{n,\theta}(\theta,\phi), \mathbf{d}^{\mathrm{Rx}}_{n,\phi}(\theta,\phi), \mathbf{d}^{\mathrm{Rx}}_{n,r}(\theta,\phi))$ such that

$$\mathbf{D}^{\mathrm{Rx}}_n(\theta,\phi) = \mathbf{A}^{\mathrm{Rx}}_n\mathbf{R}_z(\phi)\mathbf{R}_y(\theta). \tag{8}$$

Suppose that the E-fields of the incident plane wave is

$$\begin{aligned}\mathbf{E}^{\mathrm{W}} &= \mathbf{D}^{\mathrm{Rx}}_n(\theta,\phi)\mathbf{E}^{\mathrm{Rx}}\\ &= E^{\mathrm{Rx}}_\theta\mathbf{d}^{\mathrm{Rx}}_{n,\theta}(\theta,\phi) + E^{\mathrm{Rx}}_\phi\mathbf{d}^{\mathrm{Rx}}_{n,\phi}(\theta,\phi),\end{aligned} \tag{9}$$

where $\mathbf{E}^{\mathrm{W}}$ is the E-field of the incident plane wave, E^{Rx}_θ and E^{Rx}_ϕ are the E-fields on the axes $\mathbf{d}^{\mathrm{Rx}}_{n,\theta}(\theta,\phi)$ and $\mathbf{d}^{\mathrm{Rx}}_{n,\phi}(\theta,\phi)$, respectively, and $\mathbf{E}^{\mathrm{Rx}} = (E^{\mathrm{Rx}}_\theta, E^{\mathrm{Rx}}_\phi, 0)^T$.

The open-circuit voltage excited at the port of rx-antenna n by the incident plane wave is

$$\begin{aligned}V^{\mathrm{Rx}}_n &= \mathbf{L}_n(\theta,\phi)^T\mathbf{E}^{\mathrm{Rx}}\\ &= L_{n,\theta}(\theta,\phi)E^{\mathrm{Rx}}_\theta + L_{n,\phi}(\theta,\phi)E^{\mathrm{Rx}}_\phi,\end{aligned} \tag{10}$$

where $L_{n,\theta}(\theta,\phi)$ and $L_{n,\phi}(\theta,\phi)$ are the effective lengths of rx-antenna n on the axes $\mathbf{d}^{\mathrm{Rx}}_{n,\theta}(\theta,\phi)$ and $\mathbf{d}^{\mathrm{Rx}}_{n,\phi}(\theta,\phi)$, respectively, and $\mathbf{L}_n(\theta,\phi) = (L_{n,\theta}(\theta,\phi), L_{n,\phi}(\theta,\phi), 0)^T$ is the effective length vector.

We make use of the reciprocity with an infinitesimal dipole antenna for calculating the effective lengths in terms of the E-field pattern. Let us assume that an infinitesimal dipole

antenna with length l is placed at distance r towards the opposite direction of $\mathbf{d}^{\mathrm{Rx}}_{n,r}(\theta,\phi)$. The direction of the current of the infinitesimal dipole antenna is the opposite direction of $\mathbf{d}^{\mathrm{Rx}}_{n,\theta}(\theta,\phi)$. Then, the E-field, induced by current I of the infinitesimal dipole antenna, at the location of rx-antenna n is

$$E^{\mathrm{Rx}}_{\theta} = j\eta\frac{kIl}{4\pi r}\exp(-jkr), \tag{11}$$

and $E^{\mathrm{Rx}}_{\phi} = 0$. By the reciprocity theorem, the voltage V^{Rx}_{n} excited by the infinitesimal dipole antenna is equal to the voltage developed at the infinitesimal dipole antenna due to current I at the port of rx-antenna n. Therefore, V^{Rx}_{n} is calculated as

$$V^{\mathrm{Rx}}_{n} = \Omega^{\mathrm{Rx}}_{n,\theta}(\pi-\theta,\pi+\phi)\frac{1}{r}\exp(-jkr)Il, \tag{12}$$

where elevation $(\pi-\theta)$ and azimuth $(\pi+\phi)$ is the opposite direction of elevation θ and azimuth ϕ. By substituting E^{Rx}_{θ} and V^{Rx}_{n} in (10) with (11) and (12), we can calculate $L_{n,\theta}(\theta,\phi)$ as

$$L_{n,\theta}(\theta,\phi) = -2j\frac{\lambda}{\eta}\Omega^{\mathrm{Rx}}_{n,\theta}(\pi-\theta,\pi+\phi), \tag{13}$$

where $\lambda = c/f$ is the free-space wavelength, c is the speed of the light, and η is the free-space impedance. Similarly, we can calculate $L_{n,\phi}(\theta,\phi)$ by placing an infinitesimal dipole antenna with the direction of the current being $\mathbf{d}^{\mathrm{Rx}}_{\phi,r}(\theta,\phi)$. Then, we have

$$L_{n,\phi}(\theta,\phi) = 2j\frac{\lambda}{\eta}\Omega^{\mathrm{Rx}}_{n,\phi}(\pi-\theta,\pi+\phi). \tag{14}$$

Finally, the effective length vector $\mathbf{L}_n(\theta,\phi)$ is given by

$$\mathbf{L}_n(\theta,\phi) = 2j\frac{\lambda}{\eta}\mathbf{K}\mathbf{\Omega}^{\mathrm{Rx}}_{n}(\pi-\theta,\pi+\phi), \tag{15}$$

where $\mathbf{K} = \begin{bmatrix} -1 & 0 & 0 \\ 0 & 1 & 0 \\ 0 & 0 & 1 \end{bmatrix}$ is the flipping matrix over the y-z plane, and $\mathbf{\Omega}^{\mathrm{Rx}}_{n}(\theta,\phi) = (\Omega^{\mathrm{Rx}}_{n,\theta}(\theta,\phi), \Omega^{\mathrm{Rx}}_{n,\phi}(\theta,\phi), 0)^T$.

III. MULTI-ANTENNA-TO-MULTI-ANTENNA RF WIRELESS POWER TRANSFER ANALYSIS

A. IMPEDANCE MATRIX BETWEEN TRANSMIT AND RECEIVE ANTENNA ARRAYS

In this subsection, we calculate the impedance matrix between transmit and receive antenna arrays. Let us focus on a pair of tx-antenna n and rx-antenna m. Suppose that all antennas in the transmit and receive antenna arrays are open-circuited except for tx-antenna n. The current at the port of tx-antenna n is I^{Tx}_{n}. We will calculate the voltage at the port of rx-antenna m (i.e., V^{Rx}_{m}), which is induced by I^{Tx}_{n}.

A vector from tx-antenna n to rx-antenna m is defined as

$$\boldsymbol{\delta}_{m,n} = (\delta_{m,n,x}, \delta_{m,n,y}, \delta_{m,n,z})^T = \mathbf{q}^{\mathrm{Rx}}_{m} - \mathbf{q}^{\mathrm{Tx}}_{n}. \tag{16}$$

The spherical coordinate representation of the vector $\boldsymbol{\delta}_{m,n}$ is

$$r_{m,n} = \|\boldsymbol{\delta}_{m,n}\|_2, \tag{17}$$

$$\theta_{m,n} = \arccos(\delta_{m,n,z}/r_{m,n}), \tag{18}$$

$$\phi_{m,n} = \arctan 2(\delta_{m,n,y}, \delta_{m,n,x}). \tag{19}$$

We can define a global radiation frame $\mathbf{F}_{m,n}$ to represent the EM wave propagation from tx-antenna n to rx-antenna m as follows:

$$\mathbf{F}_{m,n} = \mathbf{R}_z(\phi_{m,n})\mathbf{R}_y(\theta_{m,n}). \tag{20}$$

We obtain the local radiation frame of tx-antenna n, which has the same propagation direction as $\mathbf{F}_{m,n}$. To this end, we solve the following equation to obtain three Euler angles, $\theta^{\mathrm{Tx}}_{m,n}$, $\phi^{\mathrm{Tx}}_{m,n}$, and $\psi^{\mathrm{Tx}}_{m,n}$.

$$(\mathbf{A}^{\mathrm{Tx}}_{n})^{-1}\mathbf{F}_{m,n} = \mathbf{R}_z(\phi^{\mathrm{Tx}}_{m,n})\mathbf{R}_y(\theta^{\mathrm{Tx}}_{m,n})\mathbf{R}_z(\psi^{\mathrm{Tx}}_{m,n}). \tag{21}$$

The right hand side of (21) is actually a rotation matrix corresponding to the z-y-z extrinsic rotation of the Euler angle $(\psi^{\mathrm{Tx}}_{m,n}, \theta^{\mathrm{Tx}}_{m,n}, \phi^{\mathrm{Tx}}_{m,n})$.

We define the following function Υ that converts a given rotation matrix to an Euler angle.

$$(\psi,\theta,\phi) = \Upsilon(\mathbf{X}), \tag{22}$$

where $\mathbf{X} = [X_{i,j}]$ is a 3-by-3 rotation matrix and (ψ,θ,ϕ) is the Euler angle corresponding to $\mathbf{X}$. The function Υ calculates the Euler angle from $\mathbf{X}$ as follows. We calculate θ first as $\theta = \arccos(X_{3,3})$. If $0 < \theta < \pi$, we have

$$\psi = \arctan 2(X_{3,2}, -X_{3,1}),\ \phi = \arctan 2(X_{2,3}, X_{1,3}), \tag{23}$$

and otherwise, if $\theta = 0$ or π, we have

$$\psi = \arctan 2(X_{2,1}, X_{2,2}),\ \phi = 0. \tag{24}$$

Then, the Euler angle $(\psi^{\mathrm{Tx}}_{m,n}, \theta^{\mathrm{Tx}}_{m,n}, \phi^{\mathrm{Tx}}_{m,n})$ can be calculated by using Υ as follows:

$$(\psi^{\mathrm{Tx}}_{m,n}, \theta^{\mathrm{Tx}}_{m,n}, \phi^{\mathrm{Tx}}_{m,n}) = \Upsilon((\mathbf{A}^{\mathrm{Tx}}_{n})^{-1}\mathbf{F}_{m,n}). \tag{25}$$

From (6), the local radiation frame that points towards rx-antenna m is

$$\mathbf{D}^{\mathrm{Tx}}_{n}(\theta^{\mathrm{Tx}}_{m,n}, \phi^{\mathrm{Tx}}_{m,n}) = \mathbf{A}^{\mathrm{Tx}}_{n}\mathbf{R}_z(\phi^{\mathrm{Tx}}_{m,n})\mathbf{R}_y(\theta^{\mathrm{Tx}}_{m,n}). \tag{26}$$

From (21) and (26), the relationship between the global and local radiation frames is

$$\mathbf{D}^{\mathrm{Tx}}_{n}(\theta^{\mathrm{Tx}}_{m,n}, \phi^{\mathrm{Tx}}_{m,n}) = \mathbf{F}_{m,n}\mathbf{R}_z(-\psi^{\mathrm{Tx}}_{m,n}). \tag{27}$$

From (7) and (27), the E-field of the plane wave, at the location of rx-antenna m, induced by current I^{Tx}_{n} at the port of tx-antenna n, is

$$\mathbf{E}^{\mathrm{W}}_{n}(\mathbf{q}^{\mathrm{Rx}}_{m}) = \mathbf{F}_{m,n}\mathbf{R}_z(-\psi^{\mathrm{Tx}}_{m,n})\mathbf{\Omega}^{\mathrm{Tx}}_{n}(\theta^{\mathrm{Tx}}_{m,n}, \phi^{\mathrm{Tx}}_{m,n}) \times\frac{1}{r_{m,n}}\exp(-jkr_{m,n})\cdot I^{\mathrm{Tx}}_{n}. \tag{28}$$

The local radiation frame at rx-antenna m, which describes the plane wave from tx-antenna n, is

$$\mathbf{D}^{\mathrm{Rx}}_{m}(\theta^{\mathrm{Rx}}_{m,n}, \phi^{\mathrm{Rx}}_{m,n}) = \mathbf{A}^{\mathrm{Rx}}_{m}\mathbf{R}_z(\phi^{\mathrm{Rx}}_{m,n})\mathbf{R}_y(\theta^{\mathrm{Rx}}_{m,n}), \tag{29}$$

where the Euler angle $(\psi^{\mathrm{Rx}}_{m,n}, \theta^{\mathrm{Rx}}_{m,n}, \phi^{\mathrm{Rx}}_{m,n})$ is given by

$$(\psi^{\mathrm{Rx}}_{m,n}, \theta^{\mathrm{Rx}}_{m,n}, \phi^{\mathrm{Rx}}_{m,n}) = \Upsilon((\mathbf{A}^{\mathrm{Rx}}_{m})^{-1}\mathbf{F}_{m,n}). \tag{30}$$

In addition, the local radiation frame at rx-antenna m has the following relationship with the global radiation frame.

$$\mathbf{D}_m^{\mathrm{Rx}}(\theta_{m,n}^{\mathrm{Tx}}, \phi_{m,n}^{\mathrm{Rx}}) = \mathbf{F}_{m,n}\mathbf{R}_z(-\psi_{m,n}^{\mathrm{Rx}}). \tag{31}$$

From (9), (10), (28), and (31), the voltage at the port of rx-antenna m is given by

$$\begin{aligned} V_m^{\mathrm{Rx}} &= \mathbf{L}_n(\theta_{m,n}^{\mathrm{Rx}}, \phi_{m,n}^{\mathrm{Rx}})^T(\mathbf{D}_m^{\mathrm{Rx}}(\theta_{m,n}^{\mathrm{Tx}}, \phi_{m,n}^{\mathrm{Rx}}))^{-1}\mathbf{E}_n^{\mathrm{W}}(\mathbf{q}_m^{\mathrm{Rx}}) \\ &= \mathbf{L}_n(\theta_{m,n}^{\mathrm{Rx}}, \phi_{m,n}^{\mathrm{Rx}})^T\mathbf{R}_z(\psi_{m,n}^{\mathrm{Rx}} - \psi_{m,n}^{\mathrm{Tx}})\mathbf{\Omega}_n^{\mathrm{Tx}}(\theta_{m,n}^{\mathrm{Tx}}, \phi_{m,n}^{\mathrm{Tx}}) \\ &\quad \times \frac{1}{r_{m,n}}\exp(-jkr_{m,n}) \cdot I_n^{\mathrm{Tx}}. \end{aligned} \tag{32}$$

Since all other antenna ports are open-circuited except for tx-antenna n, we have $V_m^{\mathrm{Rx}} = Z_{m,n}^{\mathrm{RT}} I_n^{\mathrm{Tx}}$. Therefore, from (32) and (15), we can finally calculate the impedance $Z_{m,n}^{\mathrm{RT}}$ as

$$\begin{aligned} Z_{m,n}^{\mathrm{RT}} &= \mathbf{\Omega}_n^{\mathrm{Rx}}(\pi - \theta_{m,n}^{\mathrm{Rx}}, \pi + \phi_{m,n}^{\mathrm{Rx}})^T \\ &\quad \times \mathbf{K}\mathbf{R}_z(\psi_{m,n}^{\mathrm{Rx}} - \psi_{m,n}^{\mathrm{Tx}})\mathbf{\Omega}_n^{\mathrm{Tx}}(\theta_{m,n}^{\mathrm{Tx}}, \phi_{m,n}^{\mathrm{Tx}}) \\ &\quad \times \frac{2j\lambda}{\eta r_{m,n}}\exp(-jkr_{m,n}). \end{aligned} \tag{33}$$

We can completely derive the impedance matrix $\mathbf{Z}^{\mathrm{RT}}$ by calculating (33) for all m and n.

B. MULTI-PORT-TO-MULTI-PORT POWER WAVE

The full impedance matrix between the transmit and receive antenna arrays in (3) can be constructed from the results in Section III-A. Now, we derive the transferrable power from the transmit to receive antenna ports based on the impedance matrix. The transmit and receive circuits are attached to the transmit and receive antenna arrays, generating and consuming the RF power, respectively. The RF power is transferred from the multiple transmit antenna ports to the multiple receive antenna ports. Although the ports of the transmit or receive circuit can be coupled, the traditional power wave concept can only describe the power transfer between decoupled ports. Thus, in this paper, we extend the power wave concept to the general multi-port-to-multi-port models as in the following.

We define the reference impedance matrices for the transmit and receive circuits as an N^{Tx}-by-N^{Tx} matrix $\mathbf{\Phi}^{\mathrm{Tx}}$ and an N^{Rx}-by-N^{Rx} matrix $\mathbf{\Phi}^{\mathrm{Rx}}$, respectively. The power waves going into the transmit and receive circuits have the impedance matrices of $\mathbf{\Phi}^{\mathrm{Tx}}$ and $\mathbf{\Phi}^{\mathrm{Rx}}$, respectively, while the power waves going out of the transmit and receive circuits have the impedance matrices of $(\mathbf{\Phi}^{\mathrm{Tx}})^H$ and $(\mathbf{\Phi}^{\mathrm{Rx}})^H$, respectively. The reference impedance matrices $\mathbf{\Phi}^{\mathrm{Tx}}$ and $\mathbf{\Phi}^{\mathrm{Rx}}$ are symmetric due to the reciprocity of the transmit and receive circuits, that is, $\mathbf{\Phi}^{\mathrm{Tx}} = (\mathbf{\Phi}^{\mathrm{Tx}})^T$ and $\mathbf{\Phi}^{\mathrm{Rx}} = (\mathbf{\Phi}^{\mathrm{Rx}})^T$. The real part of $\mathbf{\Phi}^{\mathrm{Tx}}$ and $\mathbf{\Phi}^{\mathrm{Rx}}$ (i.e., $\mathrm{Re}[\mathbf{\Phi}^{\mathrm{Tx}}]$ and $\mathrm{Re}[\mathbf{\Phi}^{\mathrm{Rx}}]$) are positive definite matrices, and therefore, the inverses of the square roots of $\mathrm{Re}[\mathbf{\Phi}^{\mathrm{Tx}}]$ and $\mathrm{Re}[\mathbf{\Phi}^{\mathrm{Rx}}]$ exist.

The incident power wave (i.e., $\mathbf{U}^{\mathrm{Tx}+}$) and the reflected power wave (i.e., $\mathbf{U}^{\mathrm{Tx}-}$) at transmit antenna ports are defined as

$$\mathbf{U}^{\mathrm{Tx}+} = \frac{1}{2}\boldsymbol{\kappa}^{\mathrm{Tx}}(\mathbf{V}^{\mathrm{Tx}} + \mathbf{\Phi}^{\mathrm{Tx}}\mathbf{I}^{\mathrm{Tx}}), \tag{34}$$

$$\mathbf{U}^{\mathrm{Tx}-} = \frac{1}{2}\boldsymbol{\kappa}^{\mathrm{Tx}}(\mathbf{V}^{\mathrm{Tx}} - (\mathbf{\Phi}^{\mathrm{Tx}})^H\mathbf{I}^{\mathrm{Tx}}), \tag{35}$$

where $\boldsymbol{\kappa}^{\mathrm{Tx}} = (\mathrm{Re}[\mathbf{\Phi}^{\mathrm{Tx}}])^{-\frac{1}{2}}$ is the inverse of the square root of the matrix $\mathrm{Re}[\mathbf{\Phi}^{\mathrm{Tx}}]$. Similarly, we also define the power waves at receive antenna ports as

$$\mathbf{U}^{\mathrm{Rx}+} = \frac{1}{2}\boldsymbol{\kappa}^{\mathrm{Rx}}(\mathbf{V}^{\mathrm{Rx}} + \mathbf{\Phi}^{\mathrm{Rx}}\mathbf{I}^{\mathrm{Rx}}), \tag{36}$$

$$\mathbf{U}^{\mathrm{Rx}-} = \frac{1}{2}\boldsymbol{\kappa}^{\mathrm{Rx}}(\mathbf{V}^{\mathrm{Rx}} - (\mathbf{\Phi}^{\mathrm{Rx}})^H\mathbf{I}^{\mathrm{Rx}}), \tag{37}$$

where $\boldsymbol{\kappa}^{\mathrm{Rx}} = (\mathrm{Re}[\mathbf{\Phi}^{\mathrm{Tx}}])^{-\frac{1}{2}}$.

By simple manipulation, we can obtain the voltages and currents at the transmit and receive antenna ports as

$$\mathbf{V}^{\mathrm{Tx}} = (\mathbf{\Phi}^{\mathrm{Tx}})^H\boldsymbol{\kappa}^{\mathrm{Tx}}\mathbf{U}^{\mathrm{Tx}+} + \mathbf{\Phi}^{\mathrm{Tx}}\boldsymbol{\kappa}^{\mathrm{Tx}}\mathbf{U}^{\mathrm{Tx}-}, \tag{38}$$

$$\mathbf{I}^{\mathrm{Tx}} = \boldsymbol{\kappa}^{\mathrm{Tx}}\mathbf{U}^{\mathrm{Tx}+} - \boldsymbol{\kappa}^{\mathrm{Tx}}\mathbf{U}^{\mathrm{Tx}-}, \tag{39}$$

$$\mathbf{V}^{\mathrm{Rx}} = (\mathbf{\Phi}^{\mathrm{Rx}})^H\boldsymbol{\kappa}^{\mathrm{Rx}}\mathbf{U}^{\mathrm{Rx}+} + \mathbf{\Phi}^{\mathrm{Rx}}\boldsymbol{\kappa}^{\mathrm{Rx}}\mathbf{U}^{\mathrm{Rx}-}, \tag{40}$$

$$\mathbf{I}^{\mathrm{Rx}} = \boldsymbol{\kappa}^{\mathrm{Rx}}\mathbf{U}^{\mathrm{Rx}+} - \boldsymbol{\kappa}^{\mathrm{Rx}}\mathbf{U}^{\mathrm{Rx}-}. \tag{41}$$

The power at the transmit antenna ports is given, in terms of the power waves, as

$$P^{\mathrm{Tx}} = \frac{1}{2}\mathrm{Re}[(\mathbf{V}^{\mathrm{Tx}})^H\mathbf{I}^{\mathrm{Tx}}] = P^{\mathrm{Tx}+} - P^{\mathrm{Tx}-}, \tag{42}$$

where $P^{\mathrm{Tx}+} = \|\mathbf{U}^{\mathrm{Tx}+}\|^2/2$ and $P^{\mathrm{Tx}-} = \|\mathbf{U}^{\mathrm{Tx}-}\|^2/2$ are the power flowing into and out of the transmit antenna ports, respectively. Similarly, the power at the receive antenna ports is given by

$$P^{\mathrm{Rx}} = P^{\mathrm{Rx}+} - P^{\mathrm{Rx}-}, \tag{43}$$

where $P^{\mathrm{Rx}+} = \|\mathbf{U}^{\mathrm{Rx}+}\|^2/2$ and $P^{\mathrm{Rx}-} = \|\mathbf{U}^{\mathrm{Rx}-}\|^2/2$ are the power flowing into and out of the receive antenna ports, respectively. Here, the power emitted from the transmit circuit is represented by the power wave $\mathbf{U}^{\mathrm{Tx}+}$, and the power received by the receive circuit is represented by the power wave $\mathbf{U}^{\mathrm{Rx}-}$.

C. POWER WAVE EQUATION FROM IMPEDANCE MATRIX

In this subsection, we calculate the relationship between the power waves from the current-voltage relationship in (3). We substitute $\mathbf{V}^{\mathrm{Tx}}$, $\mathbf{I}^{\mathrm{Tx}}$, $\mathbf{V}^{\mathrm{Rx}}$, and $\mathbf{I}^{\mathrm{Rx}}$ in (3) with (38)–(41) to obtain the following equality:

$$\mathbf{U}^{-} = \boldsymbol{\kappa}^{-1}\mathbf{\Delta}\boldsymbol{\kappa}\mathbf{U}^{+}, \tag{44}$$

where $\mathbf{\Delta} = (\mathbf{Z} + \mathbf{\Phi})^{-1}(\mathbf{Z} - \mathbf{\Phi}^H)$,

$$\mathbf{U}^{+} = \begin{bmatrix} \mathbf{U}^{\mathrm{Tx}+} \\ \mathbf{U}^{\mathrm{Rx}+} \end{bmatrix}, \quad \mathbf{U}^{-} = \begin{bmatrix} \mathbf{U}^{\mathrm{Tx}-} \\ \mathbf{U}^{\mathrm{Rx}-} \end{bmatrix}, \tag{45}$$

and

$$\mathbf{Z} = \begin{bmatrix} \mathbf{Z}^{\mathrm{TT}} & \mathbf{Z}^{\mathrm{TR}} \\ \mathbf{Z}^{\mathrm{RT}} & \mathbf{Z}^{\mathrm{RR}} \end{bmatrix}, \mathbf{\Phi} = \begin{bmatrix} \mathbf{\Phi}^{\mathrm{Tx}} & \mathbf{0} \\ \mathbf{0} & \mathbf{\Phi}^{\mathrm{Rx}} \end{bmatrix}, \boldsymbol{\kappa} = \begin{bmatrix} \boldsymbol{\kappa}^{\mathrm{Tx}} & \mathbf{0} \\ \mathbf{0} & \boldsymbol{\kappa}^{\mathrm{Rx}} \end{bmatrix}. \tag{46}$$

We can calculate $\mathbf{\Delta}$, by the block-wise matrix inversion, as follows:

$$\mathbf{\Delta} = \begin{bmatrix} \mathbf{\Delta}^{\mathrm{TT}} & \mathbf{\Delta}^{\mathrm{TR}} \\ \mathbf{\Delta}^{\mathrm{RT}} & \mathbf{\Delta}^{\mathrm{RR}} \end{bmatrix}, \tag{47}$$

where

$$\mathbf{\Delta}^{\mathrm{TT}} = (\mathbf{Z}^{\mathrm{TT}} + \mathbf{\Phi}^{\mathrm{Tx}} - \mathbf{\Gamma}^{\mathrm{Rx}})^{-1}(\mathbf{Z}^{\mathrm{TT}} - (\mathbf{\Phi}^{\mathrm{Tx}})^{H} - \mathbf{\Gamma}^{\mathrm{Rx}}), \quad (48)$$

$$\mathbf{\Delta}^{\mathrm{RT}} = (\mathbf{Z}^{\mathrm{RR}} + \mathbf{\Phi}^{\mathrm{Rx}} - \mathbf{\Gamma}^{\mathrm{Tx}})^{-1}\mathbf{Z}^{\mathrm{RT}}(\mathbf{J} - \mathbf{\Psi}^{\mathrm{Tx}}), \quad (49)$$

$$\mathbf{\Delta}^{\mathrm{TR}} = (\mathbf{Z}^{\mathrm{TT}} + \mathbf{\Phi}^{\mathrm{Tx}} - \mathbf{\Gamma}^{\mathrm{Rx}})^{-1}\mathbf{Z}^{\mathrm{TR}}(\mathbf{J} - \mathbf{\Psi}^{\mathrm{Rx}}), \quad (50)$$

$$\mathbf{\Delta}^{\mathrm{RR}} = (\mathbf{Z}^{\mathrm{RR}} + \mathbf{\Phi}^{\mathrm{Rx}} - \mathbf{\Gamma}^{\mathrm{Tx}})^{-1}(\mathbf{Z}^{\mathrm{RR}} - (\mathbf{\Phi}^{\mathrm{Rx}})^{H} - \mathbf{\Gamma}^{\mathrm{Tx}}), \quad (51)$$

$$\mathbf{\Psi}^{\mathrm{Tx}} = (\mathbf{Z}^{\mathrm{TT}} + \mathbf{\Phi}^{\mathrm{Tx}})^{-1}(\mathbf{Z}^{\mathrm{TT}} - (\mathbf{\Phi}^{\mathrm{Tx}})^{H}), \quad (52)$$

$$\mathbf{\Psi}^{\mathrm{Rx}} = (\mathbf{Z}^{\mathrm{RR}} + \mathbf{\Phi}^{\mathrm{Rx}})^{-1}(\mathbf{Z}^{\mathrm{RR}} - (\mathbf{\Phi}^{\mathrm{Rx}})^{H}), \quad (53)$$

$$\mathbf{\Gamma}^{\mathrm{Tx}} = \mathbf{Z}^{\mathrm{RT}}(\mathbf{Z}^{\mathrm{TT}} + \mathbf{\Phi}^{\mathrm{Tx}})^{-1}\mathbf{Z}^{\mathrm{TR}} \quad (54)$$

$$\mathbf{\Gamma}^{\mathrm{Rx}} = \mathbf{Z}^{\mathrm{TR}}(\mathbf{Z}^{\mathrm{RR}} + \mathbf{\Phi}^{\mathrm{Rx}})^{-1}\mathbf{Z}^{\mathrm{RT}}, \quad (55)$$

and $\mathbf{J}$ is the identity matrix. Here, $\mathbf{\Gamma}^{\mathrm{Tx}}$ in (54) and $\mathbf{\Gamma}^{\mathrm{Rx}}$ in (55) contain both $\mathbf{Z}^{\mathrm{RT}}$ and $\mathbf{Z}^{\mathrm{TR}}$, and explain the power scattered back and forth between the transmit and receive antenna arrays. In this paper, we assume that $\mathbf{\Gamma}^{\mathrm{Tx}}$ and $\mathbf{\Gamma}^{\mathrm{Rx}}$ are zero for the following reasons. First, the power received by the receive antenna array can be perfectly absorbed without backscattering if there exists a ground plane [21]. In this case, the scattered wave from the receive antenna array is canceled out by the reflected wave from the ground plane. Second, the terms containing both $\mathbf{Z}^{\mathrm{RT}}$ and $\mathbf{Z}^{\mathrm{TR}}$ are negligibly small when the transmit and receive antenna arrays are sufficiently separated.

Since the power wave from the receive circuit is zero (i.e., $\mathbf{U}^{\mathrm{Rx}+} = \mathbf{0}$), the power wave received at the receive circuit from the transmit circuit is calculated as

$$\mathbf{U}^{\mathrm{Rx}-} = \mathbf{S} \cdot \mathbf{U}^{\mathrm{Tx}+}, \quad (56)$$

where

$$\mathbf{S} = (\boldsymbol{\kappa}^{\mathrm{Rx}})^{-1}\mathbf{\Delta}^{\mathrm{RT}}\boldsymbol{\kappa}^{\mathrm{Tx}}. \quad (57)$$

D. OPTIMAL POWER WAVE FOR MAXIMIZING WIRELESS POWER TRANSFER EFFICIENCY

In this subsection, we calculate the power wave $\mathbf{U}^{\mathrm{Tx}+}$ that maximizes the power transfer efficiency. If we assume that the reference impedance matrices are perfectly matched to the mutual coupling matrix (i.e., $\mathbf{\Phi}^{\mathrm{Tx}} = (\mathbf{Z}^{\mathrm{TT}})^{H}$ and $\mathbf{\Phi}^{\mathrm{Rx}} = (\mathbf{Z}^{\mathrm{RR}})^{H}$), for example, by decoupling circuits for the antenna array, $\mathbf{S}$ can be simplified to

$$\mathbf{S} = \boldsymbol{\kappa}^{\mathrm{Rx}}\mathbf{Z}^{\mathrm{RT}}\boldsymbol{\kappa}^{\mathrm{Tx}}/2. \quad (58)$$

From (56), the transmit and receive powers are given as follows.

$$P^{\mathrm{Tx}+} = \|\mathbf{U}^{\mathrm{Tx}+}\|^2/2 = (\mathbf{U}^{\mathrm{Tx}+})^{H}\mathbf{U}^{\mathrm{Tx}+}/2, \quad (59)$$

$$P^{\mathrm{Rx}-} = \|\mathbf{U}^{\mathrm{Rx}-}\|^2/2 = (\mathbf{U}^{\mathrm{Rx}-})^{H}\mathbf{U}^{\mathrm{Rx}-}/2 = (\mathbf{U}^{\mathrm{Tx}+})^{H}\mathbf{\Theta}\mathbf{U}^{\mathrm{Tx}+}/2, \quad (60)$$

where $\mathbf{\Theta} = \mathbf{S}^{H}\mathbf{S}$. The power transfer efficiency η is given by

$$\eta = \frac{P^{\mathrm{Rx}-}}{P^{\mathrm{Tx}+}} = \frac{(\mathbf{U}^{\mathrm{Tx}+})^{H}\mathbf{\Theta}\mathbf{U}^{\mathrm{Tx}+}}{(\mathbf{U}^{\mathrm{Tx}+})^{H}\mathbf{U}^{\mathrm{Tx}+}}. \quad (61)$$

The eigenvalue decomposition of $\mathbf{\Theta}$ is given by

$$\mathbf{\Theta} = \mathbf{Q}\mathbf{\Lambda}\mathbf{Q}^{H}, \quad (62)$$

where $\mathbf{\Lambda} = \mathrm{diag}(\lambda_1, \ldots, \lambda_{N^{\mathrm{Tx}}})$ is an N^{Tx}-by-N^{Tx} diagonal matrix, and $\mathbf{Q}$ is an N^{Tx}-by-N^{Tx} unitary matrix. The diagonal entries of $\mathbf{\Lambda}$ is sorted in a decreasing order, and $\mathbf{q}_n$ is the nth column vector of $\mathbf{Q}$. Then, the power transfer efficiency is maximized when $\mathbf{U}^{\mathrm{Tx}+}$ is

$$\mathbf{U}^{\mathrm{Tx}+} = \sqrt{2P^{\mathrm{Tx}+}}\mathbf{q}_1, \quad (63)$$

and the maximum power transfer efficiency is λ_1.

E. PHASED ARRAY TRANSMIT AND RECEIVE CIRCUITS

Although the fully-matched reference impedance matrix and the optimal power wave in (58) and (63) can theoretically maximize the power transfer efficiency, it is very difficult to realize the ideal transmit and receive circuits that satisfy such conditions. Therefore, in this subsection, we suggest the phased array transmit and receive circuits, which consist of a power divider and a number of phase shifters, as an implementable alternative to the ideal circuits.

The transmit circuit has $(N^{\mathrm{Tx}} + 1)$ ports, one of which is the power input port, and the other N^{Tx} ports are connected to the transmit antenna ports. All the ports are independently matched to the real-valued reference impedance Z_0. Then, the reference impedance matrix for the transmitter is the diagonal matrix with the diagonal entries of all Z_0, i.e., $\mathbf{\Phi}^{\mathrm{Tx}} = Z_0\mathbf{J}$. The power wave at the input port is denoted by U_{in}, which is divided into N^{Tx} output ports. The power wave at the transmit array is $\mathbf{U}^{\mathrm{Tx}+} = \mathbf{w}^{\mathrm{Tx}}U_{\mathrm{in}}$, where $\mathbf{w}^{\mathrm{Tx}}$ is an N^{Tx} dimensional column vector representing transmit array weights.

The receive circuit is similar to the transmit circuit, having $(N^{\mathrm{Rx}} + 1)$ ports all of which are matched to Z_0, that is, $\mathbf{\Phi}^{\mathrm{Rx}} = Z_0\mathbf{J}$. The power wave from the receive array is combined together at the output port. That is, the power wave at the output port is $U_{\mathrm{out}} = (\mathbf{w}^{\mathrm{Rx}})^{H}\mathbf{U}^{\mathrm{Rx}-}$, where $\mathbf{w}^{\mathrm{Rx}}$ is an N^{Rx} dimensional column vector representing receive array weights.

From (56), we have

$$U_{\mathrm{out}} = (\mathbf{w}^{\mathrm{Rx}})^{H}\mathbf{S}\mathbf{w}^{\mathrm{Tx}} \cdot U_{\mathrm{in}}, \quad (64)$$

where

$$\mathbf{S} = 2(\mathbf{Z}^{\mathrm{RR}}/Z_0 + \mathbf{J})^{-1}(\mathbf{Z}^{\mathrm{RT}}/Z_0)(\mathbf{Z}^{\mathrm{TT}}/Z_0 + \mathbf{J})^{-1}. \quad (65)$$

The power transfer efficiency is

$$\eta = |U_{\mathrm{out}}|^2/|U_{\mathrm{in}}|^2 = |(\mathbf{w}^{\mathrm{Rx}})^{H}\mathbf{S}\mathbf{w}^{\mathrm{Tx}}|^2. \quad (66)$$

The array weights maximizing the power transfer efficiency can be derived by the following singular value decomposition of $\mathbf{S}$:

$$\mathbf{S} = \mathbf{\Xi}^{\mathrm{Rx}}\mathbf{\Omega}(\mathbf{\Xi}^{\mathrm{Tx}})^{H}, \quad (67)$$

where $\mathbf{\Xi}^{\mathrm{Rx}}$ and $\mathbf{\Xi}^{\mathrm{Tx}}$ are the N^{Rx}-by-N^{Rx} and N^{Tx}-by-N^{Tx} unitary matrices, and $\mathbf{\Omega}$ is the N^{Rx}-by-N^{Tx} diagonal matrix with the diagonal entries sorted in a decreasing order. Let $\boldsymbol{\xi}_n^{\mathrm{Rx}} = (\xi_{n,1}^{\mathrm{Rx}}, \ldots, \xi_{n,N^{\mathrm{Rx}}}^{\mathrm{Rx}})^{T}$ and $\boldsymbol{\xi}_n^{\mathrm{Tx}} = (\xi_{n,1}^{\mathrm{Tx}}, \ldots, \xi_{n,N^{\mathrm{Tx}}}^{\mathrm{Tx}})^{T}$ denote the nth column of $\mathbf{\Xi}^{\mathrm{Rx}}$ and $\mathbf{\Xi}^{\mathrm{Tx}}$, respectively. Then,

the power transfer efficiency η is maximized when $\mathbf{w}^{\mathrm{Rx}} = \boldsymbol{\xi}_1^{\mathrm{Rx}}/\|\boldsymbol{\xi}_1^{\mathrm{Rx}}\|$ and $\mathbf{w}^{\mathrm{Tx}} = \boldsymbol{\xi}_1^{\mathrm{Tx}}/\|\boldsymbol{\xi}_1^{\mathrm{Tx}}\|$.

However, if the transmit and receive circuits are comprised of the equal-gain power divider and the phase shifters, the magnitudes of the components of $\mathbf{w}^{\mathrm{Rx}}$ and $\mathbf{w}^{\mathrm{Tx}}$ are fixed, that is, $\mathbf{w}^{\mathrm{Rx}} = (\exp(j\theta_1^{\mathrm{Rx}})/\sqrt{N^{\mathrm{Rx}}}, \ldots, \exp(j\theta_{N^{\mathrm{Rx}}}^{\mathrm{Rx}})/\sqrt{N^{\mathrm{Rx}}})^T$ and $\mathbf{w}^{\mathrm{Tx}} = (\exp(j\theta_1^{\mathrm{Tx}})/\sqrt{N^{\mathrm{Tx}}}, \ldots, \exp(j\theta_{N^{\mathrm{Tx}}}^{\mathrm{Tx}})/\sqrt{N^{\mathrm{Tx}}})^T$. In this case, the suboptimal solution is to set $\theta_n^{\mathrm{Rx}} = \angle\xi_{1,n}^{\mathrm{Rx}}$ and $\theta_n^{\mathrm{Tx}} = \angle\xi_{1,n}^{\mathrm{Tx}}$ for all n.

F. SUMMARY OF PROPOSED ANALYSIS METHOD

In this subsection, we provide the step-by-step procedure for the proposed analysis methods as a summary of the mathematical derivations so far.

1) The input parameters are antenna positions ($\mathbf{q}_n^{\mathrm{Tx}}$ and $\mathbf{q}_m^{\mathrm{Rx}}$), antenna frames ($\mathbf{A}_n^{\mathrm{Tx}}$ and $\mathbf{A}_m^{\mathrm{Rx}}$), mutual impedance matrices ($\mathbf{Z}^{\mathrm{TT}}$ and $\mathbf{Z}^{\mathrm{RR}}$), and E-field radiation patterns ($\Omega_{n,\theta}^{\mathrm{Tx}}(\theta,\phi)$, $\Omega_{n,\phi}^{\mathrm{Tx}}(\theta,\phi)$, $\Omega_{n,\theta}^{\mathrm{Rx}}(\theta,\phi)$, and $\Omega_{n,\phi}^{\mathrm{Rx}}(\theta,\phi)$).
2) Calculate the distance $r_{m,n}$ from (17), and the global radiation frame $\mathbf{F}_{m,n}$ from (20) between tx-antenna n and rx-antenna m.
3) Derive $\psi_{m,n}^{\mathrm{Tx}}$, $\theta_{m,n}^{\mathrm{Tx}}$, and $\phi_{m,n}^{\mathrm{Tx}}$ from (25) and $\psi_{m,n}^{\mathrm{Rx}}$, $\theta_{m,n}^{\mathrm{Rx}}$, and $\phi_{m,n}^{\mathrm{Rx}}$ from (30).
4) Calculate the impedance matrix $\mathbf{Z}^{\mathrm{RT}}$ from (33) by using $r_{m,n}$, $\psi_{m,n}^{\mathrm{Tx}}$, $\theta_{m,n}^{\mathrm{Tx}}$, $\phi_{m,n}^{\mathrm{Tx}}$, $\psi_{m,n}^{\mathrm{Rx}}$, $\theta_{m,n}^{\mathrm{Rx}}$, and $\phi_{m,n}^{\mathrm{Rx}}$ obtained from steps 2) and 3).
5) In the case of optimal solution, calculate the S-parameter matrix $\mathbf{S}$ from (58), and compute the eigenvalue decomposition of $\boldsymbol{\Theta} = \mathbf{S}^H\mathbf{S}$ in (62) for deriving the optimal power wave $\mathbf{U}^{\mathrm{Tx}+}$ in (63).
6) In the case of phased array transmit and receive circuits, calculate the S-parameter matrix $\mathbf{S}$ from (65), and compute the singular value decomposition of $\mathbf{S}$ in (67) for deriving the optimal transmit and receive array weights $\mathbf{w}^{\mathrm{Tx}}$ and $\mathbf{w}^{\mathrm{Rx}}$.

IV. NUMERICAL AND EXPERIMENTAL RESULT

In this section, we compare the analytic results with the results from the full-wave EM simulator and testbed experiments for validating the proposed analysis.

A 64 antennas-to-16 antennas RF WPT system with phased array circuits (as in Section III-E) is built for the experiments. The operation frequency of the implemented RF WPT system is 5.8 GHz. We have designed and fabricated phased array boards and antenna boards as in Fig. 2(a). The phased array board has one RF port that is divided by a four-stage Wilkinson divider into 16 RF paths. In each RF path, a 6-bit digital phase shifter (Analog Device HMC1133LP5E) shifts the phase of the wave and an RF switch (Qorvo QPC6014) turns on and off the RF path. Both chips are controlled by the digital input from the shift registers (TI SN74HC595B), which form a daisy chain to provide a serial control via the board digital I/O port.

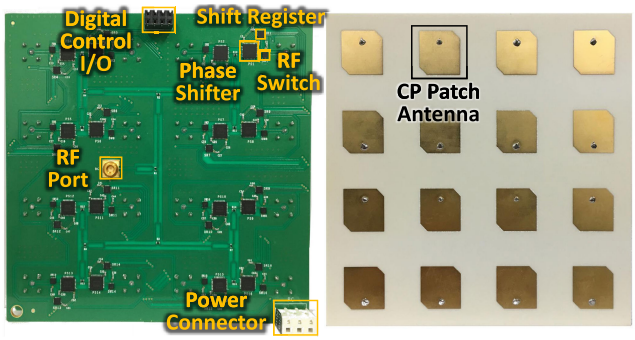

(a) Phased array and antenna boards

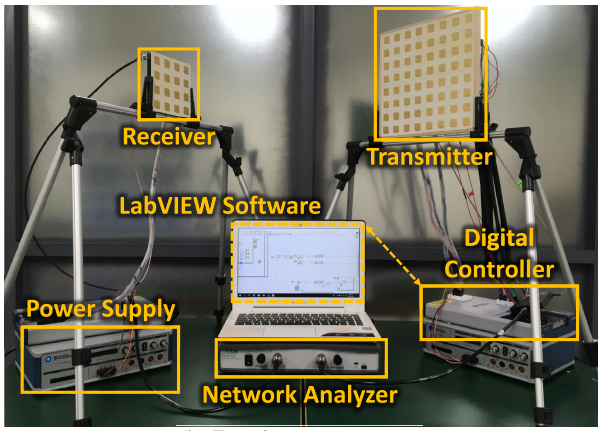

(b) Experiment system setup

FIGURE 2. Multi-antenna-to-multi-antenna RF WPT experiment system.

The antenna board is a 4-by-4 antenna array consisting of 16 circularly polarized (CP) microstrip patch antennas, fabricated on a Rogers RO4725JXR board. Each patch antenna is fed by a coaxial feed from the backside of the board, which is connected to the phased array board via Amphenol board-to-board connector. Fig. 3 shows the dimension of the microstrip patch antenna for the antenna board. The feeding point of the patch antenna is located at the distance of L_1 (4.398 mm) from the center of the patch. The dimension of the patch is $W_p = 12.75$ mm, $L_p = 12.17$ mm,

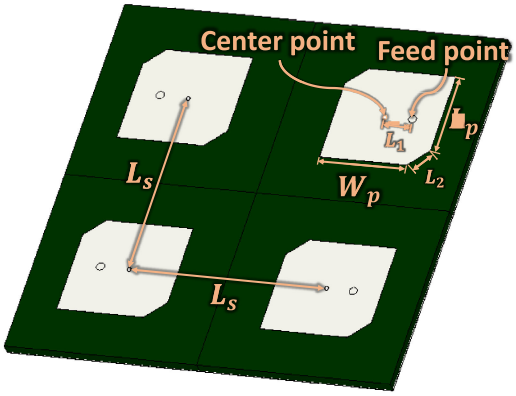

FIGURE 3. Dimension of the microstrip patch antenna.

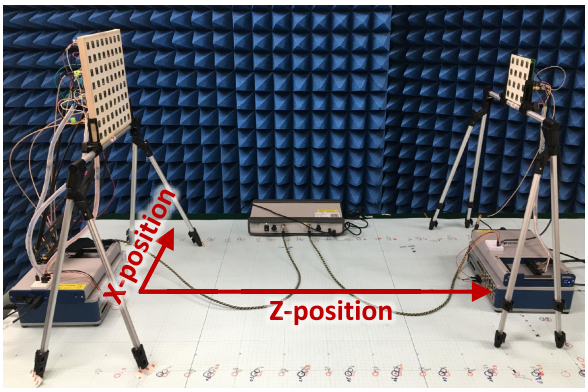

(a) Testbed setup

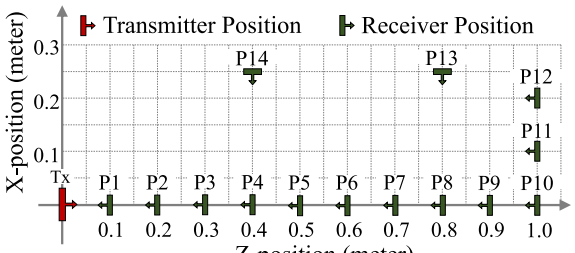

(b) Transmitter and receiver position

FIGURE 4. RF WPT testbed configuration.

and $L_2 = 3.82$ mm. The distance between the center points of neighboring antennas (L_s) is 28.2 mm.

By using the phased array and antenna boards, we have set up the RF WPT experiment system with 8-by-8 transmitter and 4-by-4 receive antenna arrays as in Fig. 2(b). Four phased array and antenna boards are combined together by a 4-way power divider to form the transmitter array. The RF ports of the transmitter and receiver are connected to the network analyzer to measure the delivery of the power wave through the RF WPT system.

We have used two software-controlled devices for controlling and measuring the RF WPT experiment system, both of which are controlled by the Labview software (version 2017) in the laptop computer. The control device is the data acquisition (DAQ) device (i.e., NI USB-6351) with 24 digital I/O pins. These I/O pins are connected to the digital I/O ports of the phased array boards of the transmitter and receiver for controlling the phase shifters. The DAQ device is directly controlled by the Labview software in the laptop through the USB connection. The measurement device is the 2-port vector network analyzer (i.e., Anritsu MS46122B) that measures the EM wave at the input RF port of the transmitter and the output RF port of the receiver. The network analyzer is controlled by the software provided by the manufacturer (i.e., Anritsu Shockline application software), which is again controlled by the Labview software via the standard commands for programmable instruments (SCPI) protocol.

Therefore, the LabVIEW software in the laptop computer can obtain the S-parameter measurements from the network analyzer, and can control the phase shifters of the transmitter and receiver. This system can calculate the

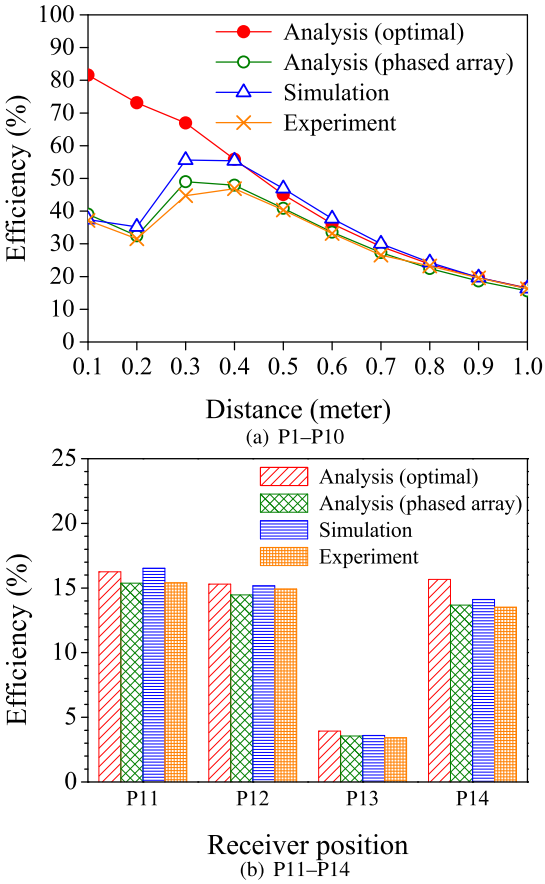

FIGURE 5. Power transfer efficiency.

S-parameter matrix (i.e., $\mathbf{S}$) between transmitter and receiver antenna ports, defined in (65). For this calculation, the network analyzer measurements for various orthogonal transmit and receive array weights are obtained, and then the S-parameter matrix is calculated by matrix inversion. From this S-parameter matrix, the optimal array weights maximizing the power transfer efficiency are derived based on the method given in Section III-E. Then, the power transfer efficiency is measured by the network analyzer when the optimal array weights are set.

We have set up the testbed as shown in Fig. 4(a), and have conducted the experiments with 14 different receiver positions, each of which is marked from P1 to P14, as given in Fig. 4(b). The receiver positions P1 to P10 correspond to the increasing distance between the transmitter and receiver from 0.1 to 1 meter. P11 and P12 describe the offset of the receiver from the center line, and P13 and P14 describe the change of the receiver direction. For the analysis and simulation, we have used exactly the same scenarios for comparison with experimental results.

For the full-wave EM simulation, we have used the time-domain solver of CST Microwave Studio running on the workstation with two NVIDIA Quadro GV100 GPUs. Even with GPU acceleration, it takes more than four days to finish the simulation of one scenario, whereas the analytic result can be derived within one second. The analytic

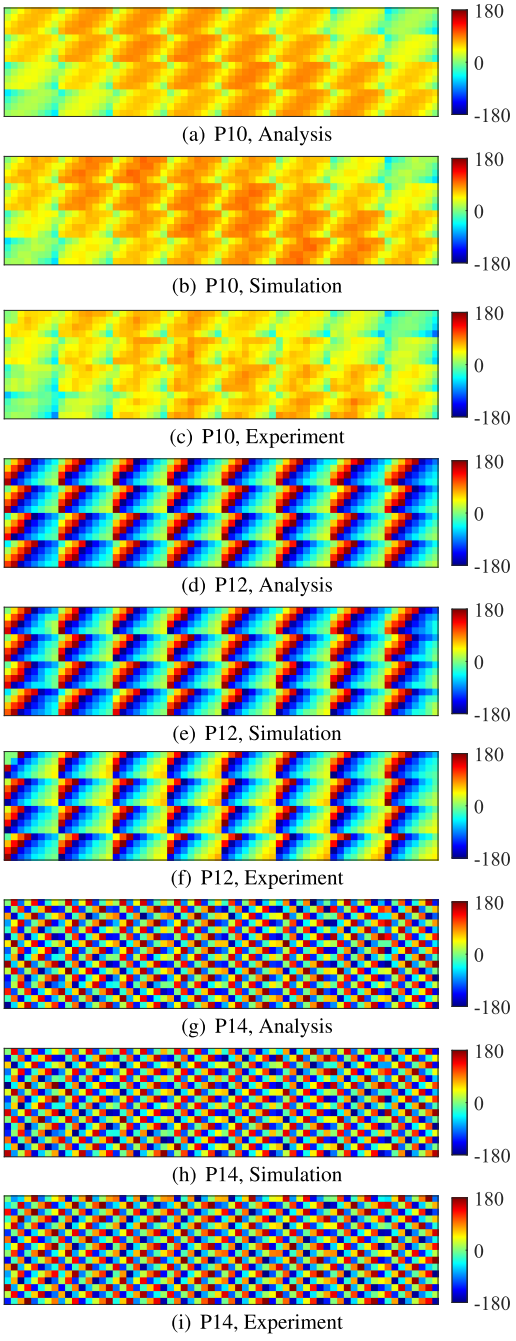

FIGURE 6. Phase of S-parameters.

equations proposed in this paper are evaluated by MATLAB. The mutual impedance matrix and radiation pattern of the antenna arrays for the analysis in Section II-C are obtained by the EM simulation and used by the MATLAB code.

Fig. 5 shows the power transfer efficiency for various receiver positions. Basically, the phased array circuit in Section III-E is applied to analysis, simulation, and experiment, and the optimal power wave result in Section III-D is obtained only by the analysis. In Fig. 5, we can see that the analytic results of the phased array circuit well agree with both the simulation and experimental results for all positions.

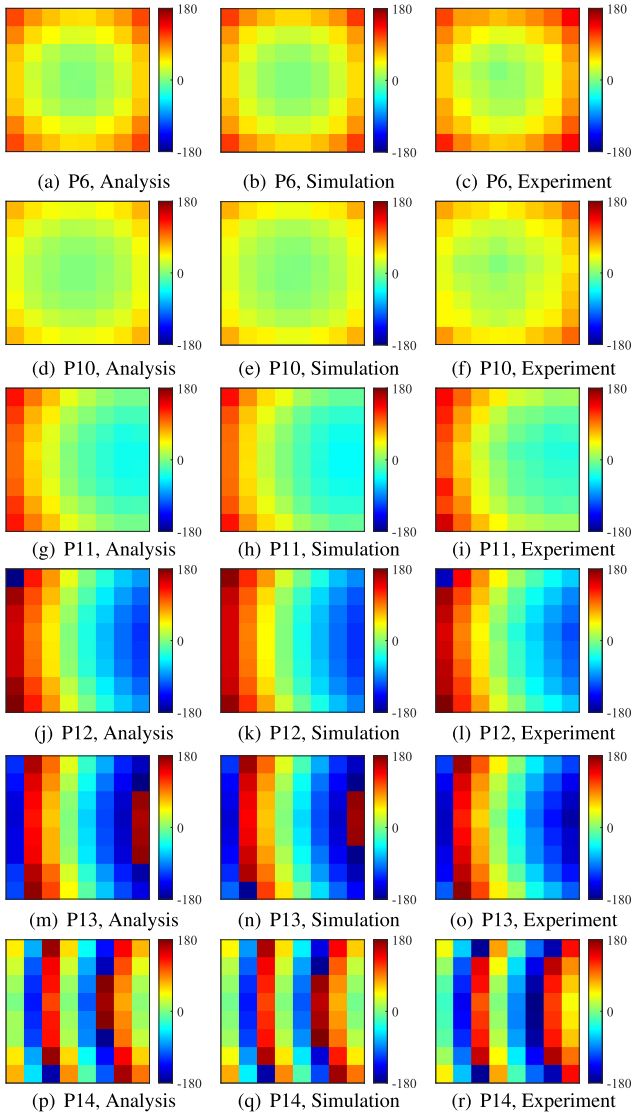

FIGURE 7. Phase of transmit array weights.

Although we have tried our best to use the same model parameters (e.g., mutual impedance matrix and radiation pattern) and testbed configuration for the analysis, simulation, and experiment, it is impossible to perfectly make all the conditions affecting the results consistent. The small discrepancy in the analysis, simulation, and experiment results in Fig. 5 could have been caused by this inconsistency.

Fig. 5(a) shows the efficiency according to the distance, i.e., at the receiver positions P1-P10. This figure shows the RF wireless power transfer within the radiative near field region rather than the far-field region since the antenna aperture size is relatively large (i.e., 64 transmit antenna elements and 16 receive antenna elements) compared to the distance only up to 1 meter. The receiver is within the radiative near field region of the transmitter if the distance is smaller than the Fraunhofer distance of the transmitter, which is defined as

$$d < \frac{2L_{\mathrm{Tx}}^2}{\lambda}, \tag{68}$$

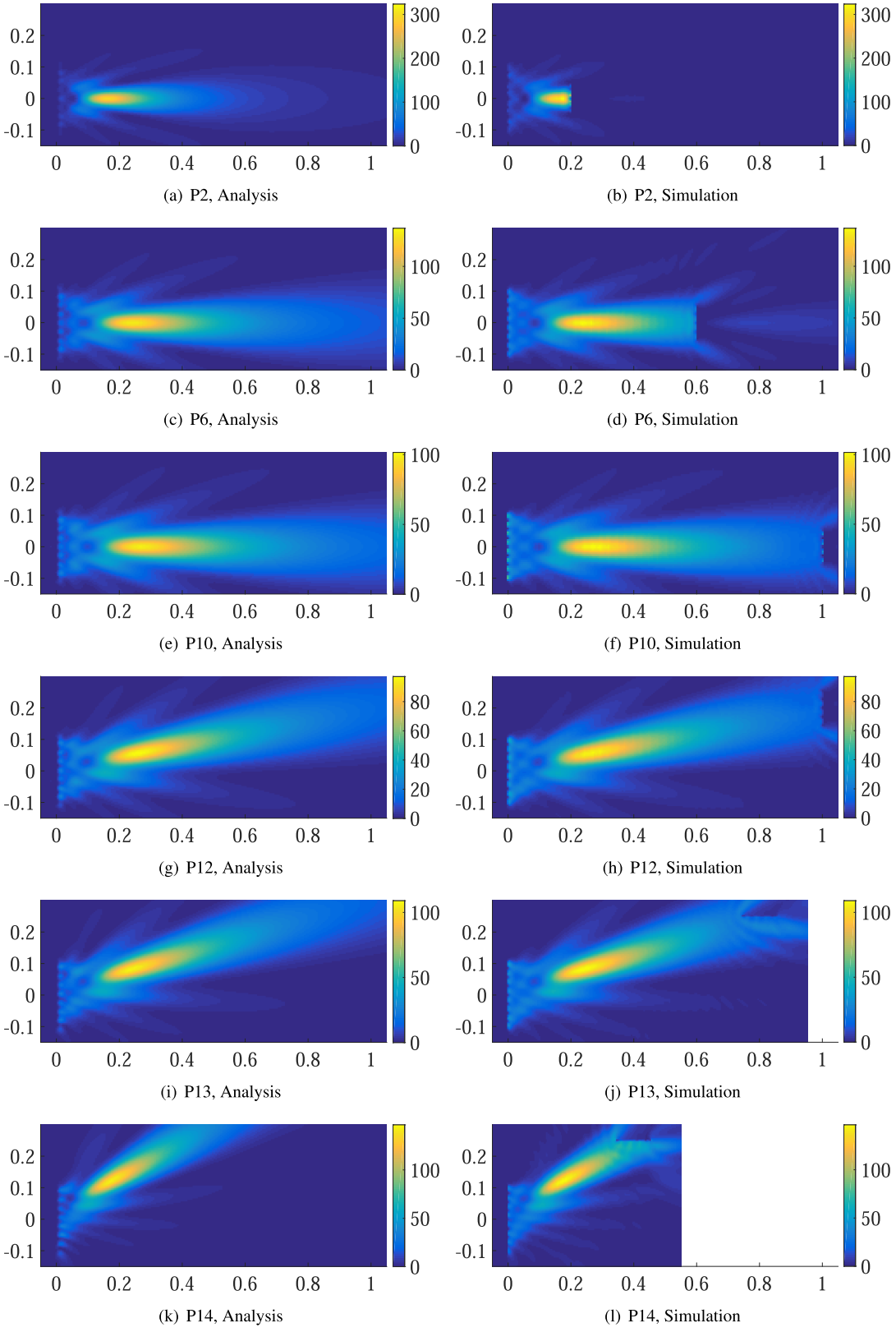

FIGURE 8. Beam shape (i.e., power density in W/m^2 over X-Z plane).

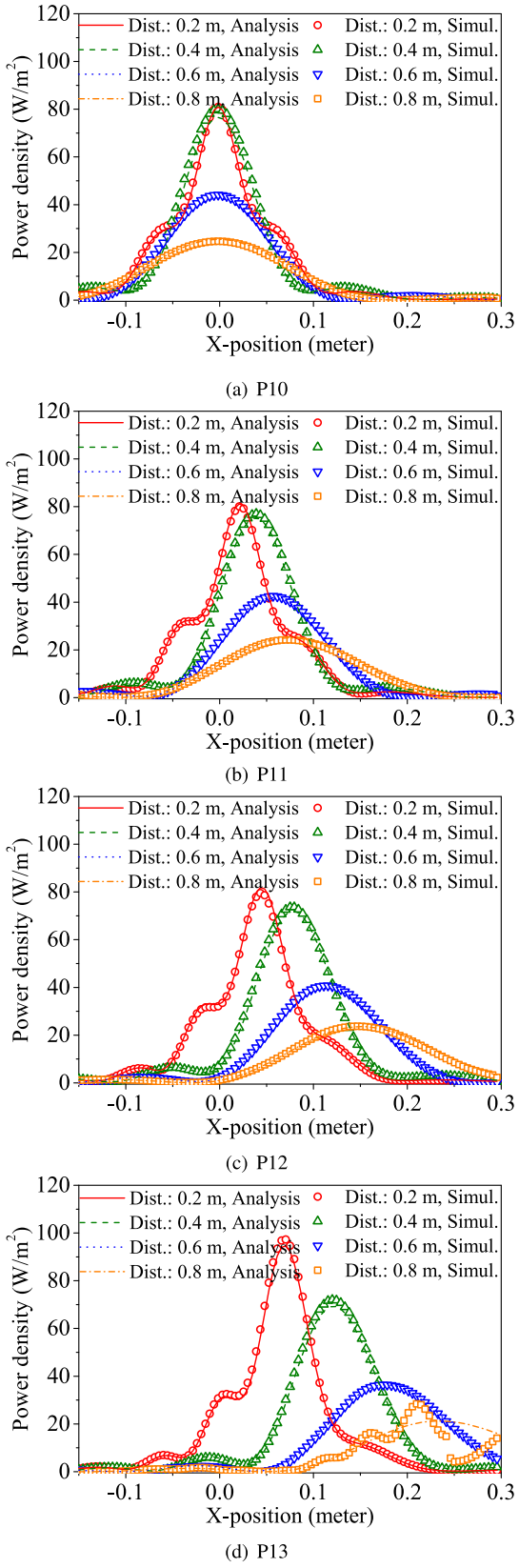

FIGURE 9. Power density profile according to distance.

where λ is the wavelength and L_{Tx} is the maximum linear dimension of the transmit antenna array. For the transmit array with 64 antennas in an 8-by-8 square form, the total size of the antenna array is 212.04 mm $\times$ 210.99 mm, the maximum linear dimension of which is 299.12 mm. Therefore, the radiative near field region is up to 3.45 meter. Since the receiver is within the radiative near field region, the plots in Fig. 5(a) do not show the trends of the inverse-square law of the Friis equation that only applies to the far-field region, and the power transfer efficiency can reach up to 80 % with the optimal power wave scheme, which is not possible in the far-field region.

In Fig. 5(a), it is seen that the analytic result of the optimal power wave scheme is the upper bound of the phased array circuit results, and monotonically increases as the receiver gets closer to the transmitter. On the other hand, the phased array circuit efficiency drops when the receiver is close to the transmitter, which is because the power radiated from the antennas around the edge of the transmitter array is wasted if the receiver is too close. The optimal power wave scheme does not have this problem since it can reduce the radiated power from the antennas around the edge in this situation. As can be seen in Fig. 5(b), the proposed analysis can predict the efficiency very well even when the transmitter and receiver do not directly face each other. The proposed analysis can be applied to any scenario with arbitrary transmitter and receiver positions and attitudes.

In the case of P13 in Fig. 5(b), the power transfer efficiency is quite low because of the following reason. In this case, the receiver antenna does not face towards the transmitter, and the distance between the transmitter and receiver is relatively large, i.e., 0.8 m. As a result, the beam from the transmitter arrives at the receiver from the side, and the reception angle of the beam is far off from the main lobe direction of the receiver antenna. This causes the beam to bounce off the receiver antenna. We will more clearly show this phenomenon in Fig. 8(j).

In Fig. 6, we compare the S-parameter matrix, defined in (65), of the analysis, simulation, and experiment at three different receiver positions. The S-parameter matrix is a 16-by-64 matrix, the phase of which is shown in the form of a heat map. We can see that the analytic result well matches with the others, and the slope of the variations in the phases of S-parameters becomes steeper as the receiver moves on to the side of the transmitter. Fig. 7 shows the phases of the transmit array weights of the analysis, simulation, and experiment. The heat map in this figure is the phase of the array weights of the 8-by-8 transmit antenna array. We can see that the convex lens-like form appears to focus the EM wave beam on to the receiver, and the focal point of the lens tracks the receiver position as the receiver moves to the side of the transmitter. It is noted that in Figs. 6 and 7, we have selectively shown

the results for a subset of receiver positions not to clutter the paper with too many graphs.

In Fig. 8, we show the beam shape of the EM wave from the transmitter, drawn by the analysis and simulation. This beam shape is actually the magnitude of the Poynting vector tangential to the Z-X plane. In the analysis, the E-field and H-field can be calculated by slightly modifying (28), and the Poynting vector is the cross product of such E-field and H-field. The power absorption at the receive antenna array is modeled in the simulation while it is not in the analysis. Except for this difference, the beam shapes of the analysis and simulation are almost identical. In this figure, we can clearly see that the beam is steered towards the receiver to maximally transfer power. From this figure, we can also get some insights into the power transfer efficiency results, for example, the efficiency decreases as the receiver moves away from the transmitter since the receiver can capture only a part of the dispersed beam. In another example, the efficiency of the P13 scenario is very low since most of the power is reflected off the receiver.

We can more clearly see that the accuracy of the beam shape of the analysis in Fig. 9 that shows the normal power going through the line, in parallel with the X-axis, lying on the X-Z plane at various distances from the transmitter. This figure shows the exact match between the beam shapes of the analysis and simulation.

V. CONCLUSION

In this paper, we have proposed the analysis method for predicting the power transfer efficiency of the RF WPT systems. We have verified the accuracy of the proposed analysis by comparing it with the experiment and full-wave EM simulation. While the full-wave simulation takes days to compute the efficiency, the proposed analysis can yield the results almost instantly. This fast analysis is very useful in designing the RF WPT systems since one can quickly evaluate the efficiency for various antenna array designs and transmitter/receiver positions and attitudes.

REFERENCES

[1] N. Shinohara, "Power without wires," *IEEE Microw. Mag.*, vol. 12, no. 7, pp. S64–S73, Dec. 2011.
[2] X. Lu, P. Wang, D. Niyato, D. I. Kim, and Z. Han, "Wireless networks with RF energy harvesting: A contemporary survey," *IEEE Commun. Surveys Tuts.*, vol. 17, no. 2, pp. 757–789, 2nd Quart., 2015.
[3] K. Dang, J. Zhang, H. Zhou, S. Yin, T. Zhang, J. Ning, Y. Zhang, Z. Bian, J. Chen, X. Duan, S. Zhao, and Y. Hao, "Lateral GaN Schottky barrier diode for wireless high-power transfer application with high RF/DC conversion efficiency: From circuit construction and device technologies to system demonstration," *IEEE Trans. Ind. Electron.*, vol. 67, no. 8, pp. 6597–6606, Aug. 2020.
[4] L. Guo, X. Gu, P. Chu, S. Hemour, and K. Wu, "Collaboratively harvesting ambient radiofrequency and thermal energy," *IEEE Trans. Ind. Electron.*, vol. 67, no. 5, pp. 3736–3746, May 2020.
[5] W. Lin and R. W. Ziolkowski, "Electrically small, single-substrate huygens dipole rectenna for ultra-compact wireless power transfer applications," *IEEE Trans. Antennas Propag.*, early access, Jul. 1, 2020, doi: 10.1109/TAP.2020.3004987.
[6] A. Massa, G. Oliveri, F. Viani, and P. Rocca, "Array designs for long-distance wireless power transmission: State-of-the-Art and innovative solutions," *Proc. IEEE*, vol. 101, no. 6, pp. 1464–1481, Jun. 2013.
[7] Y. Li and V. Jandhyala, "Design of retrodirective antenna arrays for short-range wireless power transmission," *IEEE Trans. Antennas Propag.*, vol. 60, no. 1, pp. 206–211, Jan. 2012.
[8] M. Ettorre, W. A. Alomar, and A. Grbic, "2-D van atta array of wideband, wideangle slots for radiative wireless power transfer systems," *IEEE Trans. Antennas Propag.*, vol. 66, no. 9, pp. 4577–4585, Sep. 2018.
[9] G. Oliveri, L. Poli, and A. Massa, "Maximum efficiency beam synthesis of radiating planar arrays for wireless power transmission," *IEEE Trans. Antennas Propag.*, vol. 61, no. 5, pp. 2490–2499, May 2013.
[10] K. W. Choi, L. Ginting, A. A. Aziz, D. Setiawan, J. H. Park, S. I. Hwang, D. S. Kang, M. Y. Chung, and D. I. Kim, "Toward realization of long-range wireless-powered sensor networks," *IEEE Wireless Commun.*, vol. 26, no. 4, pp. 184–192, Aug. 2019.
[11] Q. Hui, K. Jin, and X. Zhu, "Directional radiation technique for maximum receiving power in microwave power transmission system," *IEEE Trans. Ind. Electron.*, vol. 67, no. 8, pp. 6376–6386, Aug. 2020.
[12] D. Belo, D. C. Ribeiro, P. Pinho, and N. Borges Carvalho, "A selective, tracking, and power adaptive far-field wireless power transfer system," *IEEE Trans. Microw. Theory Techn.*, vol. 67, no. 9, pp. 3856–3866, Sep. 2019.
[13] K. Zhang, C. Liu, Z. H. Jiang, Y. Zhang, X. Liu, H. Guo, and X. Yang, "Near-field wireless power transfer to deep-tissue implants for biomedical applications," *IEEE Trans. Antennas Propag.*, vol. 68, no. 2, pp. 1098–1106, Feb. 2020.
[14] S. Yu, H. Liu, and L. Li, "Design of near-field focused metasurface for high-efficient wireless power transfer with multifocus characteristics," *IEEE Trans. Ind. Electron.*, vol. 66, no. 5, pp. 3993–4002, May 2019.
[15] H.-T. Chou, "Conformal near-field focus radiation from phased array of antennas to enhance power transfer between transmitting and receiving antennas," *IEEE Trans. Antennas Propag.*, vol. 68, no. 5, pp. 3567–3577, May 2020.
[16] R. Gonzalez Ayestaran, G. Leon, M. R. Pino, and P. Nepa, "Wireless power transfer through simultaneous near-field focusing and far-field synthesis," *IEEE Trans. Antennas Propag.*, vol. 67, no. 8, pp. 5623–5633, Aug. 2019.
[17] G. Borgiotti, "Maximum power transfer between two planar apertures in the fresnel zone," *IEEE Trans. Antennas Propag.*, vol. 14, no. 2, pp. 158–163, Mar. 1966.
[18] J.-H. Kim, Y. Lim, and S. Nam, "Efficiency bound of radiative wireless power transmission using practical antennas," *IEEE Trans. Antennas Propag.*, vol. 67, no. 8, pp. 5750–5755, Aug. 2019.
[19] T. A. Khan, A. Yazdan, and R. W. Heath, Jr., "Optimization of power transfer efficiency and energy efficiency for wireless-powered systems with massive MIMO," *IEEE Trans. Wireless Commun.*, vol. 17, no. 11, pp. 7159–7172, Nov. 2018.
[20] S. Zhong and X. Wang, "Wireless power transfer by beamspace large-scale MIMO with lens antenna array," *IEEE Trans. Wireless Commun.*, vol. 18, no. 2, pp. 1390–1403, Feb. 2019.
[21] D.-H. Kwon and D. M. Pozar, "Optimal characteristics of an arbitrary receive antenna," *IEEE Trans. Antennas Propag.*, vol. 57, no. 12, pp. 3720–3727, Dec. 2009.

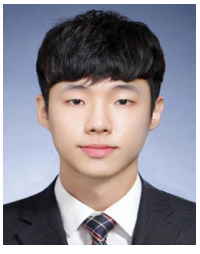

JE HYEON PARK (Student Member, IEEE) received the B.S. degree from the School of Electronic and Electronic and Electrical Engineering, Sungkyunkwan University, Suwon, South Korea, in 2018, where he is currently pursuing the Ph.D. degree. His current research interests include radio frequency circuit design and antenna array signal processing.

DONG IN KIM (Fellow, IEEE) received the Ph.D. degree in electrical engineering from the University of Southern California, Los Angeles, CA, USA, in 1990. He was a tenured Professor with the School of Engineering Science, Simon Fraser University, Burnaby, BC, Canada. Since 2007, he has been an SKKU-Fellowship Professor with the College of Information and Communication Engineering, Sungkyunkwan University (SKKU), Suwon, South Korea. He is a Fellow of the Korean Academy of Science and Technology, and a member of the National Academy of Engineering of Korea. He has been a first recipient of the NRF of Korea Engineering Research Center in Wireless Communications for RF Energy Harvesting, since 2014. He was a 2019 recipient of the IEEE Communications Society Joseph LoCicero Award for Exemplary Service to Publications. He is the Executive Chair of IEEE ICC 2022, Seoul. He has been listed as a 2020 Highly Cited Researcher by Clarivate Analytics. From 2001 to 2020, he served as an Editor and the Editor-at-Large of Wireless Communication I for the IEEE TRANSACTION ON COMMUNICATIONS. From 2002 to 2011, he also served as an Editor and a Founding Area Editor of Cross-Layer Design and Optimization for the IEEE TRANSACTIONS ON WIRELESS COMMUNICATIONS. From 2008 to 2011, he served as the Co-Editor-in-Chief for the IEEE/KICS JOURNAL ON COMMUNICATIONS AND NETWORKS. He served as the Founding Editor-in-Chief for the IEEE WIRELESS COMMUNICATIONS LETTERS, from 2012 to 2015.

KAE WON CHOI (Senior Member, IEEE) received the B.S. degree in civil, urban, and geosystem engineering and the M.S. and Ph.D. degrees in electrical engineering and computer science from Seoul National University, Seoul, South Korea, in 2001, 2003, and 2007, respectively. From 2008 to 2009, he was with Telecommunication Business of Samsung Electronics Company Ltd., South Korea. From 2009 to 2010, he was a Postdoctoral Researcher with the Department of Electrical and Computer Engineering, University of Manitoba, Winnipeg, MB, Canada. From 2010 to 2016, he was an Assistant Professor with the Department of Computer Science and Engineering, Seoul National University of Science and Technology, South Korea. In 2016, he joined the faculty at Sungkyunkwan University, South Korea, where he is currently an Associate Professor with the College of Information and Communication Engineering. His research interests include RF energy transfer, metasurface communication, visible light communication, cellular communication, cognitive radio, and radio resource management. He has been serving as an Editor for IEEE COMMUNICATIONS SURVEYS & TUTORIALS, since 2014, for IEEE WIRELESS COMMUNICATIONS LETTERS, since 2015, for IEEE TRANSACTIONS ON WIRELESS COMMUNICATIONS, since 2017, and for IEEE TRANSACTIONS ON COGNITIVE COMMUNICATIONS AND NETWORKING, since 2019.